DINAME 2023 - Proceedings of the XIX International Symposium on Dynamic Problems of Mechanics,
A.S. De Paula, A.T. Fabro and M.R. Machado (Editors), ABCM.
Pirenópolis, Go, Brazil, February 26th to March 3rd, 2023

Reconstructing nanoscale topography using a controlled vibrating fiber and iterative model inversion

Izhak Bucher [1] and Eyal Baruch [1]

[1] Technion Israel Institute of technology, Department of Mechanical Engineering, Haifa 3200003, Israel

Abstract: Measuring Nanoscale topography presents a great challenge to microelectronics industries. Presented is a method to reconstruct the topography of surface contours in inaccessible regions without contact, exploiting the intermolecular forces between a vibrating fiber and the measured surface. In small scales the Van der Waals (VdW) interaction forces produce measurable changes and in larger scale, magnetic interaction serves the same purpose. A vibrating Nanowire is incrementally inserted into grooves or moved along a measured surface and multiple measurements are combined to reconstruct the measured topography. A nonlinear inverse problem is solved iteratively after performing an automatic calibration stage. Simulated examples are provided for magnetic and VdW forces alongside large-scale experiment with magnetic forces.

Keywords: Topography reconstruction, Inverse problem, Nonlinear force identification, Autoresonance

INTRODUCTION

The present paper introduces a solve an inverse problem with which the topography of barely accessible surfaces can be reconstructed. This method utilizes the interaction forces between a vibrating fiber and the measured surface which to find the surface topography. In small scales, where Van der Waals (VdW) interactions between a sensing tip or fiber and the measured sample prevail, the dynamics of a vibrating fiber are affected by these forces. The latter is exploited in Atomic force microscopes (AFM) [1] and and the change in the natural frequencies of the system [2] due to change in the overall potential affected by the spacing of interacting molecules in the sensor and specimen. In order to overcome these limitations, different methods were introduced. CD AFM, or 3D AFM uses a boot shaped tip to improve resolution and measure sidewalls [3]. Tilted AFM uses one or two tilted cantilevers to achieve better resolution of the critical dimensions [4]. Furthermore, different types of tips were used to obtain better resolution, such as flared tips [5], and nanowires [6]. Still, these methods have some limitations due to the approximation method, the assumption that the tip interacts with a single point of the topography, and the size of the tip itself [7].

In order to deal with distributed interactions, an iterative method of approximation was developed. This method replaces the set of nonlinear coupled equations with a set of solvable equations, by iteratively updating the equations up to convergence.

Since nanowire sensing and the AFM method are based on perturbations of the of system resonant frequency, Autoresonance (AR) was used to excite the system in resonance. The Autoresonance (AR) technique exploits a relay based nonlinear positive feedback control loop to automatically excite a specific mode of vibration of the system in resonance [8], [9].

To verify the proposed approximation method, a scaled experimental system which utilizes magnetic forces was constructed. Since the magnetic potential is a function of the distance to a certain negative power, similarly to the VdW potential, the approximation of a magnetic topography via magnetic interactions can be analogous to the exploitation of VdW interactions in AFM. While generally the magnetic potential is dependent on the orientation of the magnets [10], whereas the VdW potential is only dependent on the distance, it is possible to choose an orientation of the magnets which eliminates these unwanted effects and serves as a reasonable representation of VdW interactions.

This paper is arranged as follows: section 2 describes the dynamics of the system and constructs the set of equations that will result in the approximation of the topography, section 3 describes the iterative method for solving this set of equations, section 4 describes the method of actuation and measurement of the system, and finally, section 5 presents the experimental results, verifying the approximation method.

Underlying dynamics of the system

The objective of this manuscript is to develop a method which exploits the effects of Van der Waals interaction forces between a nanowire and a nanoscale sample, to measure the sample topography.

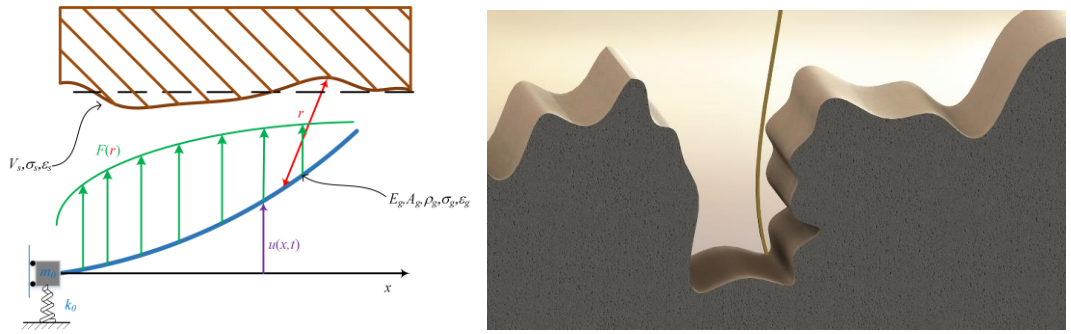

Figure 1 – The schematics of the simulated system. The nanowire (in blue) interacts with the topography sample (in brown) resulting in forces (in green), which can be translated to added stiffness which changes the natural frequency of the system.

Here $u(x,t)$ is the transverse displacement of the beam, V_s is the volume of a silicon element, and σ_s, ε_s are the material constants used for the Lennard – Jones approximation of the Van der Waals Potential [11]

$$V = -4\varepsilon_{1-2}\left(\frac{\sigma_{1-2}}{r}\right)^6 \left[kJmol^{-1}\right]. \tag{1}$$

Similarly, E_g and A_g are the Young modulus and cross-section of the gold nanowire, and σ_g, ε_g are the Gold material constants. r represents the distance between a single element of the beam and a single silicon element, and $F(r)$ represents the overall acting force on the beam due to the atomic interactions.

The displacement of the beam can be described as:

$$r_{beam} = \left(x, u_{ss}(x) + u(x)\right) \tag{2}$$

where x is a coordinate along the beam, u_{ss} is the steady state, static deflection of the beam, and u is the beam's dynamic deflection coordinate caused by an oscillating force applied to it.

The measured topography is:

$$r_t = \left(g_1(\zeta), g_2(\zeta)\right) \tag{3}$$

Where $\zeta \in [0, L_{top}]$ is a parameter along the topography. The potential between a point on the beam and differential topography element will then be:

$$dV(x) = -\frac{C}{r^n} = -\frac{C}{\left(\sqrt{\left(g_1(\zeta)-x\right)^2 + \left(g_2(\zeta)-u-u_{ss}\right)^2}\right)^n} d\zeta \tag{4}$$

where r is the distance between the topography and the beam, and $C = -4\varepsilon\sigma^6, n = 6$. The force acting on the beam will be:

$$f(x) = \int_0^{L_{top}} Cn \frac{\left(g_2(\zeta)-u-u_{ss}\right)}{\left(\sqrt{\left(g_1(\zeta)-x\right)^2 + \left(g_2(\zeta)-u-u_{ss}\right)^2}\right)^{n+2}} d\zeta \tag{5}$$

The system ODE is:

$$\rho A u_{tt} + EI u_{xxxx} = f(x) \tag{6}$$

This is a highly nonlinear ODE, since $f(x)\,f(x)$ is a function of $u\,u$ to some negative power. To be able to evaluate the system's response, a Finite Element model of the system is derived.

FINITE ELEMENT MODEL DERIVATION

Assuming the beam acts according to the Euler Bernoulli theory, the beam can be modeled using the appropriate Hermitian beam elements. Therefore, the full displacement can be described as:

$$u(x)=\sum_{j=1}^{N} H_j(x) \tag{7}$$

where $H_j(x)$ is the Hermitian function of the j_{th} element and N is the total number of elements. As a result, the displacement of the j^{th} element q_j, and it's angle θ_j can be derived.

Using virtual work, A transfer matrix Q was constructed to project $f(x)$ on to the relevant coordinates. In addition, the mass and stiffness matrices were derived using:

$$M_{r,s}=\frac{\partial^2 \frac{1}{2}\rho A\int_0^L \dot{u}(x)^2\,dx,}{\partial\dot{q}_r\partial\dot{q}_s}, K_{r,s}=\frac{\partial^2\left(\frac{1}{2}EI\int_0^L u''(x)^2\,dx\right)}{\partial q_r\partial q_s} \tag{8}$$

The EOM of the beam with Van der Waals interacting forces will be:

$$M\ddot{q}+C\dot{q}+Kq=Qf(x) \tag{9}$$

Since $f(x)$ is a function of the topography of the system, it is of interest to construct a method which utilizes $f(x)$ to extract the topography. This can be done by exciting the system in small amplitudes, and using the linearization of $f(x)$ in order to be able to extract the topography from a linear system.

LINEARIZED MODEL FOR SMALL OSCIILATIONS

The nonlinear VdW interaction force $f(x)$ affects the steady state solution of the linearized system in 2 manners: it both changes the static deflection of the beam u_{ss}, and acts as an elastic bedding, which changes the natural frequencies of the system. However, the $f(x)$ itself is a function of u_{ss} (see Eq. (5)). Therefore, in order to accurately approximate the linearized elastic bedding, u_{ss} must be first approximated.

Stiffness matrix approximation

Assuming small displacements, a linearized stiffness matrix can be derived from the potential by taking the second derivative of the potential V at equilibrium, (which is defined as $u=0$) :

$$k(x)=\left.\frac{\partial^2 V}{\partial u^2}\right|_{eq}=\int_0^{L_{top}}\left(Cn\frac{\left(g_1(\zeta)-x\right)^2-(n+1)\left(g_2(\zeta)-u_{ss}\right)^2}{\left(\sqrt{\left(g_1(\zeta)-x\right)^2+\left(g_2(\zeta)-u_{ss}\right)^2}\right)^{n+4}}\right)d\zeta\,. \tag{10}$$

This function is projected on the system coordinates using the same matrix Q resulting in:

$$K_{VdW} = Qk(x). \tag{11}$$

The EOM of the beam with Van der Waals interacting forces will be:

$$M\ddot{q} + C\dot{q} + (K + K_{VdW})q = 0 \tag{12}$$

By solving the generalized eigenvalue problem of the matrices $(M, K + K_{VdW})$ the perturbed natural frequency is obtained. Therefore, by measuring the natural frequency of the system, information regarding K_{VdW} can be obtained, and subsequently the topography $(g_1(\zeta), g_2(\zeta))$ can be approximated. However, the dependency between the natural frequencies and the topography is highly nonlinear. Using a standard gradient descent procedure to find $\mathbf{g}$ is time consuming, since $\mathbf{g}$ requires many parameters to accurately describe the topography. This necessitates the development of a nonlinear approximation method for extracting $\boldsymbol{g}(\zeta)$.

ITERATIVE TOPOGRAPHY APPROXIMATION

The approximation method is presented as a flow chart in the following figure. The proof and conditions for convergence are presented in the appendix.

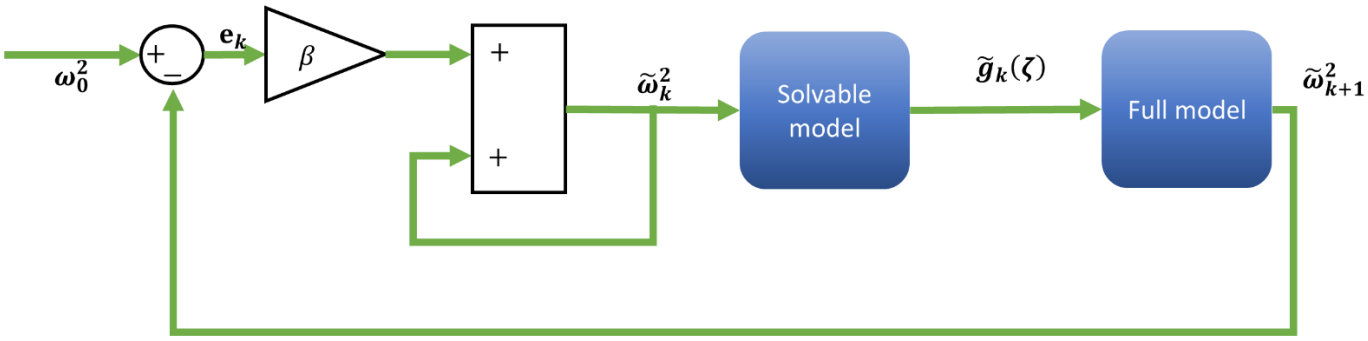

Figure 2 The flowchart of the iterative topography approximation method. The evaluation of the topography using the solvable model is plugged into the full model to update the frequency vector $\tilde{\omega}$.

The measured frequency vector $\tilde{\boldsymbol{\omega}}_{\boldsymbol{k}}$ is used to approximate the topography $\tilde{\boldsymbol{g}}_{\boldsymbol{k}}(\zeta)$ using a simplified solvable model. Using the full model approximation (see section 4) , The natural frequencies $\tilde{\boldsymbol{\omega}}_{\boldsymbol{k+1}}$ are approximated assuming the topography $\tilde{\boldsymbol{g}}_k(\zeta)$ interacts with the beam. The error $\mathbf{e}_i$ is defined as:

$$\mathbf{e}_k = \boldsymbol{\omega}_0^2 - \tilde{\boldsymbol{\omega}}_k^2 \tag{13}$$

The error multiplied by some gain β and added to $\tilde{\boldsymbol{\omega}}_{\boldsymbol{k}}$ resulting in:

$$\tilde{\boldsymbol{\omega}}_{k+1}^2 = \tilde{\boldsymbol{\omega}}_k^2 + \beta\left(\tilde{\boldsymbol{\omega}}_0^2 - \tilde{\boldsymbol{\omega}}_k^2\right) \tag{14}$$

To apply this model, a solvable set of equations is derived, assuming: 1. $\left(g_1(\zeta), g_2(\zeta)\right)$ can be presented as $\left(\tilde{g}(\zeta), \zeta\right)$ since the tip is perpendicular to the topography, 2. $g_1(\zeta)$ can be approximated as a piecewise constant function, 3. the static forces are negligible, resulting in $u_{ss} \approx 0$, resulting in:

$$k(x)=\int_0^{L_{top}}\left(Cn\frac{\left(g(\zeta)-x\right)^2(n+1)-\zeta^2}{\left(\sqrt{\left(g(\zeta)-x\right)^2+\zeta^2}\right)^{n+4}}\right)d\zeta=$$
$$\sum_{i=0}^{N-1}\int_{\frac{i}{N}L_{top}}^{\frac{i+1}{N}L_{top}}\left(Cn\frac{\left(g_i-x\right)^2(n+1)-\zeta^2}{\left(\sqrt{\left(g_i-x\right)^2+\zeta^2}\right)^{n+4}}\right)d\zeta \tag{15}$$

and the equation of motion of a beam is:

$$\rho A u_{tt}+EIu_{xxxx}-k(x)u=0 \tag{16}$$

In addition, it is assumed that $k(x)$ does not change the mode shapes significantly, resulting in:

$$u=a\phi(x) \tag{17}$$

where the mode ϕ_n is approximated to be the discretization of the analytical mode of a Euler Bernoulli beam [12]

$$X_n(x)=\cosh(\beta x)-\cos(\beta x)-\frac{\cos(\beta L_{beam})+\cosh(\beta L_{beam})}{\sin(\beta L_{beam})+\sinh(\beta L_{beam})}\left[\sinh(\beta x)-\sin(\beta x)\right] \tag{18}$$

where:

$$\beta^4=\frac{\rho A}{EI}\omega_n^2, \tag{19}$$

L_{beam} is the length of the beam, and ω_n is the natural frequency of the unperturbed system. substituting Eq. (17) in Eq. (16) results in:

$$\ddot{a}\phi+\omega_n^2 a\phi+\frac{k(x)}{\rho A}a\phi=0 \tag{20}$$

By multiplying by ϕ and integrating over the length of the beam, the following equation is obtained:

$$\ddot{a}+\left(\omega_n^2+\frac{\int_0^{L_{beam}}\phi^2 k(x)dx}{\rho A\int_0^{L_{beam}}\phi^2 dx}\right)a=0 \tag{21}$$

Indicating that the change in the natural frequency is:

$$\Delta\omega_n^2=\frac{\int_0^{L_{beam}}\phi^2(x)k(x)dx}{\rho A\int_0^{L_{beam}}\phi^2(x)dx} \tag{22}$$

Substituting Eq.(15) into Eq. (22):

$$\Delta\omega_{n,j}^2=\frac{\int_0^{L_{beam}}\phi^2(x)\sum_{i=0}^{N-1}\int_{\frac{i}{N}L_{top}}^{\frac{i+1}{N}L_{top}}\left(Cn\frac{\left(g_i-x\right)^2(n+1)-\zeta^2}{\left(\sqrt{\left(g_i-x\right)^2+\zeta^2}\right)^{n+4}}\right)d\zeta dx}{\int_0^{L_{beam}}\phi^2(x)dx} \tag{23}$$

In addition, it is assumed that the strongest interaction and most dominant is at $\zeta = 0$, which is the part of the topography which is directly parallel to the beam. This results in the set of solvable equations:

$$\Delta\omega_{n,i} = \frac{L_{top}Cn(n+1)}{N} \frac{\int_0^{L_{beam}} \frac{\phi^2(x)}{(g_i - x)^{n+2}} dx}{\int_0^{L_{beam}} \phi^2(x) dx} \tag{24}$$

Which is a set of decoupled nonlinear equations of the single parameter g_i which can be easily obtained. Therefore, by measuring the change in the natural frequency parallel to each point in the topography, resulting with vector $\boldsymbol{\Delta\omega_n}$ **(Figure 3)**.

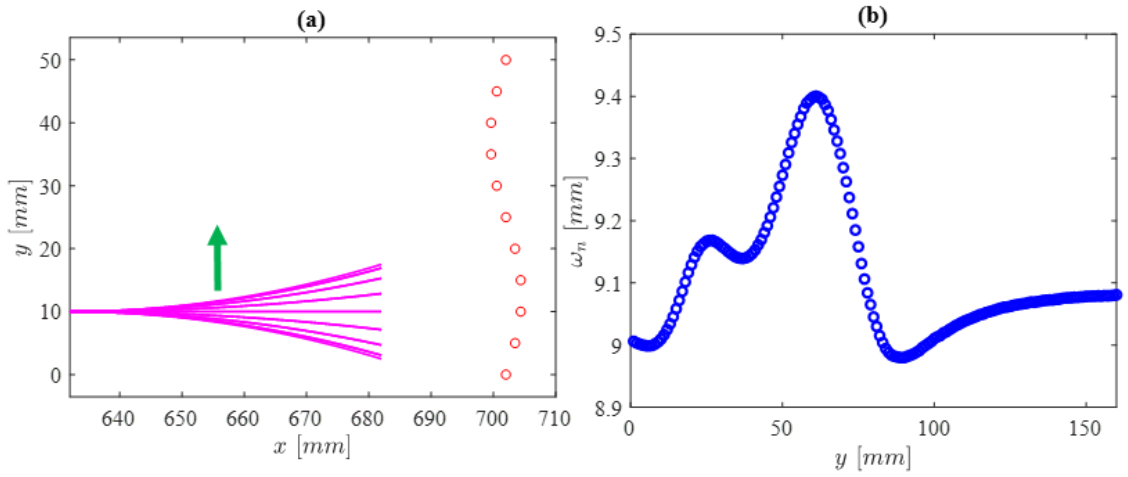

Figure 3 The approximation set. The natural frequency is measured in different points along the topography (4.a) and the measurements are collected into a vector (4.b)

The measured perturbation in the natural frequency is used for the iterative approximation method, where $\tilde{\boldsymbol{g}}$ converges to the real topography $\mathbf{g}$.

It is important to note, that to refrain from divergence of the method, the full model approximation of $\tilde{\boldsymbol{\omega}}_{\boldsymbol{k+1}}$ is implemented in 3 successive steps: first using Eq. (23) (closest to the solvable model of Eq. (24)), then solving the eigenvalue problem with the mass and stiffness matrices of Eq. (12), assuming $u_{ss} = 0$,

Experimental results

The objective of this manuscript is to develop a method which exploits the effects of Van der Waals interaction

Magnetic analogy

Magnetic forces have similar properties Van der Waals interaction forces, since in the proper configuration they are also a function of the distance by a certain power.

The interaction potential between two dipoles can be approximated as [13]:

$$V = -\frac{C}{r^3}\left(3(I_1 \cdot \hat{r})(I_2 \cdot \hat{r}) - (I_1 \cdot I_2)\right) \tag{25}$$

where C is a constant resulting from the magnetic moments and permeability, r is the distance between the two centers of the moments, $\hat{r}$ is the normalized vector in the direction of r, and I_1, I_2 are the normalized vectors in the

directions of the first and second dipoles respectively. Assuming the vectors I_1, I_2 are parallel with opposite signs, and that $\hat{r}$ is orthogonal to I_1, I_2, the force becomes:

$$V = -\frac{C}{r^3}. \tag{26}$$

These forces can be analogous to Van der Waals forces, and therefore this configuration can be used to validate the method of identification.

Test rig measured and reconstructed results

The method was verified using a magnetic system which substitutes the VdW potential with a magnetic one. The system is presented in Figure 4:

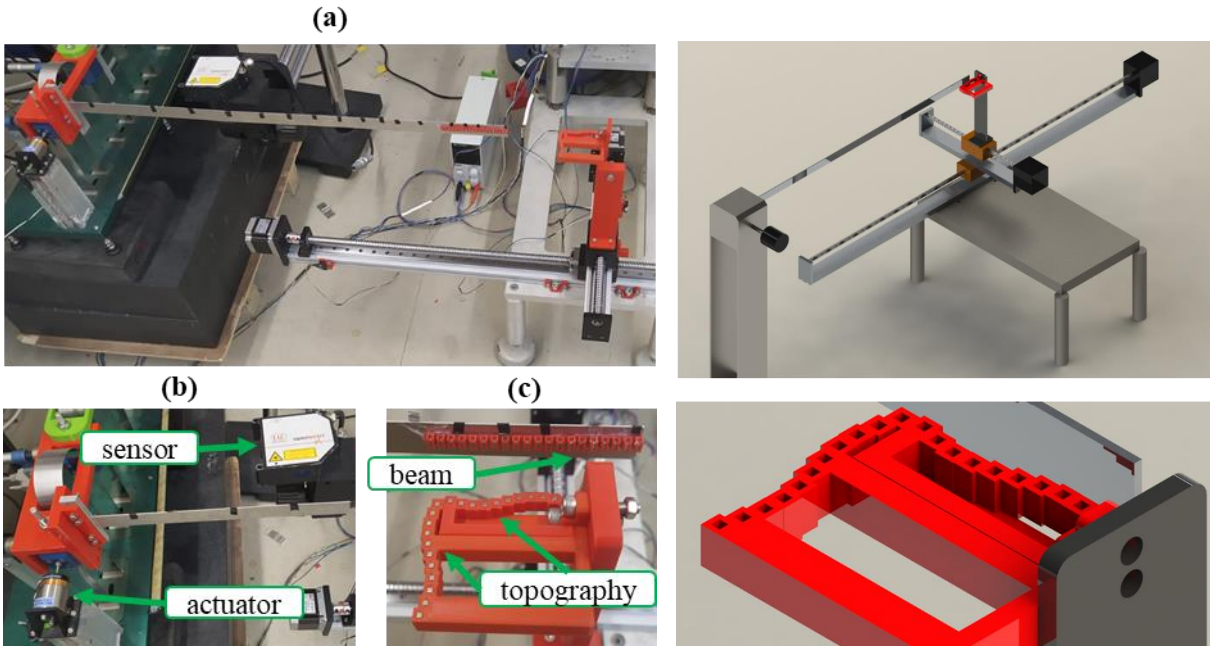

Figure 4 – The magnetic experimental system. (a) The full system. (b) The sensor that measures the beam and the actuator that resonates it. (c) The measured topography and the magnetic beam. The potential constants were calibrated, and the topography was approximated via the found potential.

Calibration set

The system was calibrated using a single magnet. The natural frequency was measured in different distances from the beam, and the values of C, n and ω_0 were approximated. The calibration set and it's approximation are presented in Figure 5:

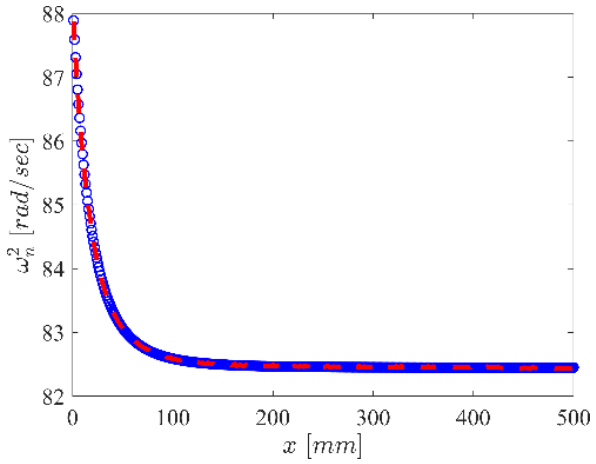

Figure 5 – The calibration set. In red – the measured set. In blue, the approximated set using the calibrated parameters.

It is evident that the error between the measured and approximated natural frequency is small, indicating of a precise approximation of C and n.

Approximation set

The approximation set was measured by moving the beam across the topography at a nominal distance of 20[mm] and measuring the natural frequency. Using the measurements, the topography was approximated:

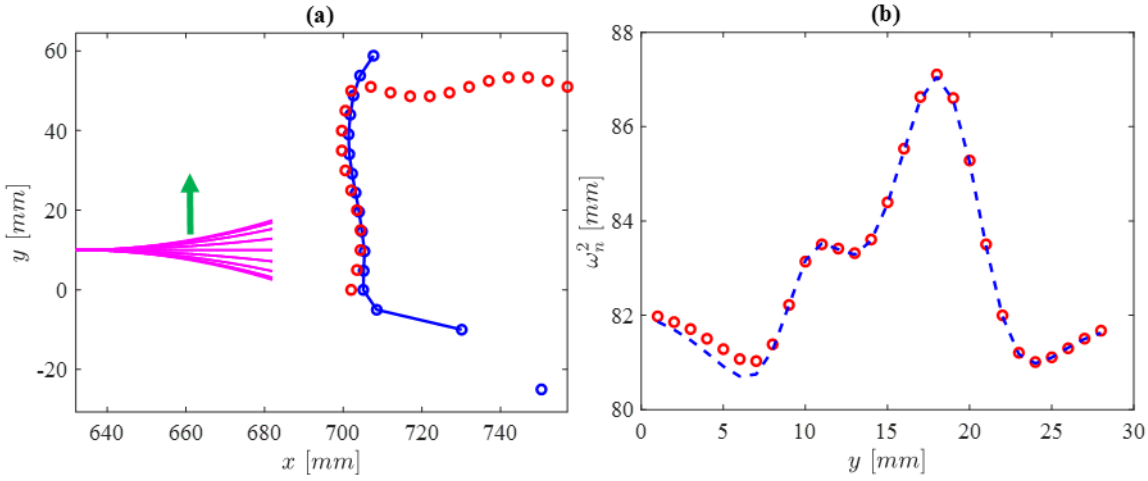

Figure 6 -The topography approximation. (a) shows the topography in red and the approximation in blue. (b) shows the measured approximation set of frequencies in red and the approximated one in blue.

Next, the beam was inserted into the area where the topography is farther away, to approximate the groove.

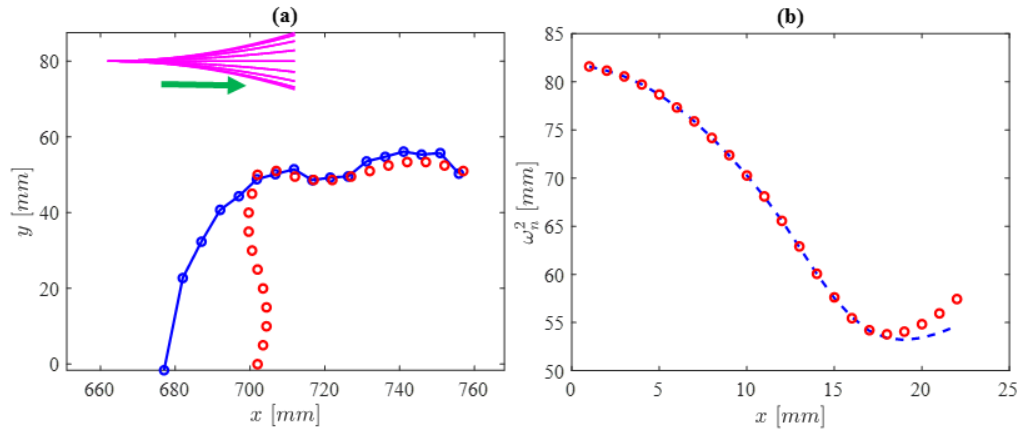

Figure 7 – The groove approximation. The beam (in red) is inserted into the groove, the natural frequencies are measured in (b) and the topography is approximated in (a).

The parts of the topography after the intersection is omitted, resulting in:

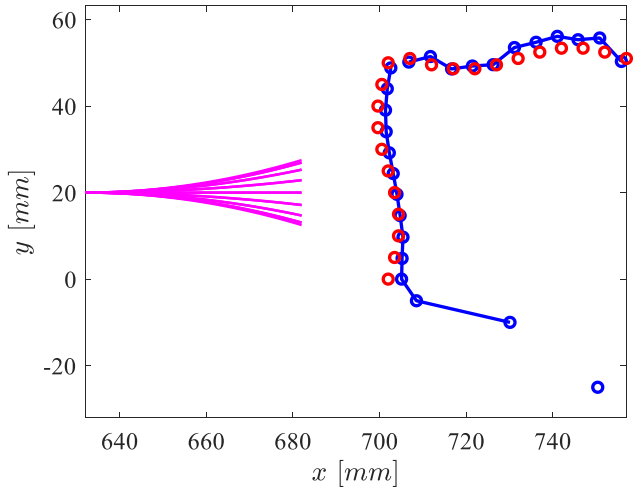

Figure 8 – The full topography of the system. The real topography is in red, and the approximated topography is in blue.

It is evident that the approximated topography reproduces the real one, and that the groove can be measured by inserting the beam.

Summary

A method for approximation of complex topographies by adding a nanowire to the tip of an AFM was proposed. The dynamics of the nanowire were described, and an iterative method for the approximation of the topography from the nonlinear equations of the natural frequency of the nanowire was formulated. The approximation method was verified using an up scaled system which substituted VdW interaction forces with magnetic ones. Experimental results validate the ability to approximate complex topographies, including grooves, with high resolution.

ACKNOWLEDGMENTS (HEADING 1, HELVETICA 11PT BOLD ALL CAPS)

The authors are thankful to Mr. Nir Ben-Shaya for his great ideas. This work was funded by the Israeli Innovation Authority within the Multi-Dimensional Metrology (MDM) consortium

REFERENCES

[1] T. R. Albrecht, P. Grütter, D. Horne, and D. Rugar, “Frequency modulation detection using high-Q cantilevers for enhanced force microscope sensitivity,” Journal of Applied Physics, 1991, doi: 10.1063/1.347347.

[2] T. R. Albrecht, P. Grütter, D. Horne, and D. Rugar, “Frequency modulation detection using high-Q cantilevers for enhanced force microscope sensitivity,” Journal of Applied Physics, 1991, doi: 10.1063/1.347347.

[3] Y. Martin and H. K. Wickramasinghe, “Method for imaging sidewalls by atomic force microscopy,” Applied Physics Letters, 1994, doi: 10.1063/1.111578.

[4] V. Mancevski and P. F. McClure, “Development of a dual-probe Caliper CD-AFM for near model-independent nanometrology,” 2002. doi: 10.1117/12.473418.

[5] D. Hussain, K. Ahmad, J. Song, and H. Xie, “Advances in the atomic force microscopy for critical dimension metrology,” Measurement Science and Technology. 2017. doi: 10.1088/0957-0233/28/1/012001.

[6] J. Choi et al., “Evaluation of carbon nanotube probes in critical dimension atomic force microscopes,” Journal of Micro/Nanolithography, MEMS, and MOEMS, 2016, doi: 10.1117/1.jmm.15.3.034005.

[7] S. Santos, V. Barcons, H. K. Christenson, J. Font, and N. H. Thomson, “The intrinsic resolution limit in the atomic force microscope: Implications for heights of nano-scale features,” PLoS ONE, 2011, doi: 10.1371/journal.pone.0023821.

[8] K. J. Aström, G. C. Goodwin, and P. R. Kumar, Adaptive control, filtering, and signal processing, vol. 150. 2012.

[9] V. I. Babitsky, “Autoresonant mechatronic systems,” Mechatronics, vol. 5, no. 5, pp. 483–495, Aug. 1995, doi: 10.1016/0957-4158(95)00026-2.

[10] W. S. Price, “Spin dynamics: Basics of nuclear magnetic resonance, 2nd edition.,” Concepts in Magnetic Resonance Part A, 2009, doi: 10.1002/cmr.a.20130.

[11] J. E. Lennard-Jones, “Cohesion,” Proceedings of the Physical Society, 1931, doi: 10.1088/0959-5309/43/5/301.

[12] M. Géradin and D. J. Rixen, Mechanical Vibrations: Theory and Application to Structural Dynamics. Chichester: John Wiley & Sons, 2015.

[13] W. S. Price, “Spin dynamics: Basics of nuclear magnetic resonance, 2nd edition.,” Concepts in Magnetic Resonance Part A, 2009, doi: 10.1002/cmr.a.20130.